THE ASTROPHYSICAL JOURNAL, 417:528–540, 1993 November 10

FAINT OBJECT CAMERA FAR-ULTRAVIOLET OBJECTIVE PRISM OBSERVATIONS OF 12 $z > 3$ QUASARS[1]

P. JAKOBSEN,[2] R. ALBRECHT,[3,4,5] C. BARBIERI,[6] J. C. BLADES,[7] A. BOKSENBERG,[8] P. CRANE,[3] J. M. DEHARVENG,[9] M. J. DISNEY,[10] T. M. KAMPERMAN,[11] I. R. KING,[12] F. MACCHETTO,[5,7] C. D. MACKAY,[13] F. PARESCE,[5,7,14] G. WEIGELT,[15] D. BAXTER,[7] P. GREENFIELD,[7] R. JEDRZEJEWSKI,[7] A. NOTA,[5,7] W. B. SPARKS[7]

Received 1993 February 11; accepted 1993 May 18

ABSTRACT

We present the first results of an exploratory objective prism survey of the far-ultraviolet ($\lambda\lambda$1200–1800) spectra of high-redshift quasars obtained with the Faint Object Camera on-board the *Hubble Space Telescope*. The prime objective of this survey is to identify one or more candidates among the known quasars at $z_{em} > 3$ with sufficient flux at far-ultraviolet wavelengths to enable detailed follow-up observations of redshifted intergalactic He II λ304 absorption using the *HST* grating spectrographs. FOC prism observations of 12 prime candidates selected for redshift ($z_{em} \simeq 3.03$–3.66), brightness ($V \lesssim 18.5$) and the appearance of their optical absorption spectra are presented and discussed. As anticipated beforehand, cumulative neutral hydrogen Lyman continuum absorption from the various classes of intervening absorption systems presents a serious obstacle for observing high redshift quasars at extreme ultraviolet rest energies. At our limiting sensitivity of $F_\lambda \simeq 2$–4×10^{-16} ergs s^{-1} cm^{-2} Å^{-1}, 10 of the 12 objects observed show no far-UV flux shortward of λ1800 observed wavelength. Two objects, Q0114−089 (UM 670; $z_{em} = 3.16$) and Q1442+102 (OQ 172; $z_{em} = 3.53$) are detected, but only down to $\lambda \simeq 330$ Å and $\lambda \simeq 345$ Å rest wavelength. No object is reliably detected at emitted He II λ304. The severity of the cumulative Lyman continuum absorption is, however, such that these preliminary findings are still statistically consistent with the hypothesis that luminous quasars are intrinsically bright at extreme ultraviolet energies at flux levels comparable to those suggested by extrapolation of the power law continua seen at longer wavelengths. A larger number of high-redshift quasars need to be observed in the far-UV before the prospects for observing intergalactic He II λ304 absorption with *HST* can be fully appraised.

Subject headings: intergalactic medium — quasars: general — surveys — ultraviolet: galaxies

1. INTRODUCTION

There are several reasons why observing the highest redshift $z_{em} > 3$ quasars at far-ultraviolet wavelengths—corresponding to emitted energies below the Lyman limit—has long been considered to be a prime task for the *Hubble Space Telescope* (*HST*). For one, the intrinsic extreme ultraviolet spectra of quasars are crucial for understanding the quasar phenomenon itself, since the ionizing photon output in this region powers the emission-line region and provides important clues as to the origin of the continuum emission (Bechtold et al. 1984; Edelson & Malkan 1986; O'Brian, Gondhalekar, & Wilson 1988; Madau 1988; Reimers et al. 1989; Courvoisier & Clavel 1991). The detection and study of extreme ultraviolet emission lines such as He I λ584 and He II λ304 are also of interest for understanding the physics of the quasar broad-line region (e.g., Davidson & Netzer 1979).

Second, and perhaps even more important, by using high-redshift quasars as far-UV background sources, the helium content of the early universe can be gauged by means of the He I λ584 and He II λ304 equivalents of the Gunn & Peterson (1965) test for intergalactic gas and by searching for narrow He I and He II absorption lines matching those seen in Lyα absorption systems in quasar spectra. Of special interest are the clouds of gas giving rise to the so-called Lyman forest systems, which are possibly of primordial composition (e.g., Sargent 1988). A measurement of the helium content of the Lyman forest clouds will provide a critical consistency check of big bang nucleosynthesis theory and yield unique information on the physical conditions in the intergalactic medium at early epochs (Sargent et al. 1980; Green et al. 1980; Sherman 1982; Ikeuchi & Ostriker 1986; Bechtold et al. 1987b; Sciama 1988; Miralda-Escudé & Ostriker 1990, 1992, and references therein).

Virtually all current theories for quasar absorption line

[1] Based on observations with the NASA/ESA *Hubble Space Telescope*, obtained at the Space Telescope Science Institute, which is operated by AURA, Inc., under NASA contract NAS 5-26555.

[2] Astrophysics Division, Space Science Department of ESA, ESTEC, 2200 AG Noordwijk, The Netherlands.
[3] European Southern Observatory, Karl Schwarzschild Strasse 2, 8046 Garching, Germany.
[4] Space Telescope European Coordinating Facility.
[5] Affiliated to the Astrophysics Division, Space Science Department of ESA.
[6] Dipartimento di Astronomia, Vicolo dell'Osservatorio 5, I-35122 Padova, Italy.
[7] Space Telescope Science Institute, 3700 Martin Drive, Baltimore, MD 21218.
[8] Royal Greenwich Observatory, Madingley Road, Cambridge CB3 0EZ, UK.
[9] Laboratoire d'Astronomie Spatiale du CNRS, Traverse du Siphon, Les Trois Lucs, 13012 Marseille, France.
[10] Department of Physics, University College of Cardiff, P.O. Box 713, Cardiff CF1 3TH, Wales, UK.
[11] Space Research Institute, Sorbonnelaan 2, 3584 CA Utrecht, The Netherlands.
[12] Astronomy Department, University of California, Berkeley, CA 94720.
[13] Institute of Astronomy, Madingley Road, Cambridge CB3 OHA, UK.
[14] Osservatorio Astronomico Torino, Strada Osservatorio 20, I-10025 Pino Torinese, Italy.
[15] Max Planck Institut für Radioastronomie, Auf dem Hügel 69, 5300 Bonn 1, Germany.

systems and the intergalactic medium predict that the helium contained in both the Lyman forest clouds and in any ambient intergalactic gas is highly ionized. Consequently, intergalactic helium is expected to be mainly observable through absorption in the He II λ304 line of once ionized helium, rather than in the He I λ584 line of neutral helium. The basis for this clear prediction and some of its possible observational consequences are outlined in the Appendix.

Notwithstanding the long-standing interest in observing He II in emission and absorption in high-redshift quasars, it is, however, not obvious that such observations are actually feasible with *HST* in practice. The He II λ304 line is redshifted sufficiently above the $\simeq\lambda$1150 MgF_2 low wavelength cutoff of the *HST* optics to be observable only in the highest redshift quasars at $z_{em} > 3$. The line of sight out to this redshift will on the average intercept some $\sim$400 Lyman forest clouds with hydrogen column densities $N_{HI} \simeq 10^{13}$–10^{17} cm^{-2} (Sargent et al. 1980; Murdoch et al. 1986; Hunstead 1988) and some $\sim$6 "Lyman limit" systems with densities $N_{HI} \simeq 10^{17}$–10^{22} cm^{-2} (Tytler 1982; Bechtold et al. 1984; Lanzetta 1988; Sargent, Steidel, & Boksenberg 1989; Bahcall et al. 1993). Photoelectric absorption in this intervening neutral hydrogen presents a serious obstacle for observing high-redshift quasars at any rest wavelength below the Lyman limit.

The statistics and radiative transfer of the Lyman continuum absorption from the two types of H I quasar absorption line systems has been discussed in detail by Møller & Jakobsen (1990). Although the Lyman forest systems are individually optically thin in the Lyman continuum, the accumulated redshift smeared absorption from the large number of such clouds intercepted leads to a characteristic "Lyman valley" shaped averaged absorption spectrum reaching an optical depth of order unity near $\sim$650 Å in the quasar rest frame. Just as all high-redshift quasars invariably show Lyman forest absorption in Lyα lines, the far-UV spectra of all high-redshift quasars will also show signs of matching Lyman valley continuum absorption. Moreover, since this absorption is the cumulative effect of many absorbers along the line of sight, only relatively modest variations in the magnitude of the Lyman forest contribution to the total absorption are expected between different objects at a given redshift.

A much more serious obstacle for observing high-redshift quasars in the far-UV is posed by Lyman continuum absorption from the $\sim$100 times scarcer, but optically thick Lyman limit class of absorption systems. The densest of such systems with H I column densities $N_{HI} \gtrsim 10^{19}$ cm^{-2} completely absorb the spectrum of any background quasar at all far-UV wavelengths below the redshifted Lyman limit of the intervening cloud, thereby making observations of helium absorption lines impossible. As opposed to the Lyman valley absorption, however, this absorption component arises in a modest number of absorbers along the line of sight and therefore exhibits very large fluctuations from object to object.

As shown by Møller & Jakobsen (1990), current statistics for the line-of-sight density, column density distribution and redshift evolution of the Lyman forest and Lyman limit types of quasar absorption systems imply that the probability of a random line of sight experiencing less than 75% total absorption at redshifted He II λ304 is of order $p_0 \simeq 5\%$–10% at $z_{em} \simeq 3$ and drops rapidly with increasing redshift to $p_0 \simeq 1\%$ at $z_{em} \simeq 4$. In other words, only a minority of $z_{em} > 3$ quasars are expected to be observable at all at far-UV wavelengths due to intervening Lyman continuum opacity.

The discovery of the UV-bright $z_{em} = 2.72$ quasar, HS 1700+6416 (Reimers et al. 1989, 1992), on the other hand, provides reason for some optimism. Although the redshift of this bright ($V \simeq 16$) object is too small to bring the He II λ304 line within reach of *HST*, its mere existence does serve to demonstrate both that at least some quasars possess intrinsically energetic extreme UV spectra and that moderately ($\simeq 50\%$) absorbed sight lines do exist out to high redshift.

A further important limitation concerns the absolute flux level for which detailed far-UV spectroscopy of the redshifted He II λ304 region is feasible in practice. The present sensitivity limit of the Faint Object Spectrograph and the Goddard High-Resolution Spectrograph on-board *HST* at S/N = 10 and 10–20 hours of integration time is approximately $F_\lambda \simeq 5 \times 10^{-16}$ ergs s^{-1} cm^{-2} Å^{-1} at $\simeq$1250 Å. This is equivalent to the flux at He II received from a $V \simeq 18$, $z_{em} \simeq 3$ quasar having an intrinsic $F_\nu \propto \nu^{-0.6}$ power-law spectrum similar to that of HS 1700+6416, attenuated by intervening absorption corresponding to a residual transmission of 25%. The first step toward observing primordial ionized helium with *HST* is to find such a "clear" object among the few hundred $z_{em} > 3$ quasars presently known. Many of the more heavily absorbed high-redshift quasars can be identified beforehand on the basis of strong Lyman absorption edges and Lyα systems seen in their optical spectra. However, this approach is not failproof because of uncertainties in the derived H I column densities and the limited redshift windows probed. At least half of all Lyman limit systems detected in the visible are expected to have $N_{HI} \lesssim 2 \times 10^{18}$ cm^{-2} and should therefore become transparent at shorter wavelengths due to the $\sigma_{HI} \propto \nu^{-3}$ dependence of the photoelectric cross section. Conversely, quasars that appear to have clear lines of sight in the optical will in many cases contain strong unseen absorption systems at lower redshift.

Given this inherently stochastic nature of the cumulative intervening absorption, the only way of finding a UV bright $z_{em} > 3$ quasar suitable for detection of He II absorption is to carry out an ultraviolet survey of a significant number of objects. In this paper we present the first results of an on-going survey of high-redshift quasars employing the far-UV objective prisms of the Faint Object Camera on-board *HST*. The aim of this survey is to gauge the far-UV fluxes of a number of high-redshift quasars in the hope of finding one or more only moderately absorbed objects bright enough for extensive follow-up observations using the *HST* UV spectrographs. Calibration exposures carried out with the FOC objective prisms in orbit have demonstrated that in spite of the factor $\approx$6 loss in sensitivity caused by the *HST* spherical aberration, the FOC prisms are still the fastest low-resolution UV spectroscopic option presently available onboard *HST*. Moreover, the fact that the FOC objective prisms can be used in a simple "point and shoot" manner makes this mode ideally suited to the problem at hand.

In this paper we present observations of 12 high-redshift objects selected for their optical brightness ($V \lesssim 18.5$), redshift ($3.0 \lesssim z \lesssim 3.7$) and appearance of their optical absorption spectra. The objects observed are listed in Table 1. Our main result is that none of the objects observed so far is detected at redshifted He II λ304 down to a limiting sensitivity of $F_\lambda \simeq 2$–4×10^{-16} ergs s^{-1} cm^{-2} Å^{-1}. Two of the objects do, however, show evidence of a weak far-UV flux at emitted wavelengths corresponding to $\lambda \gtrsim 330$ Å.

The remainder of this paper is organized as follows: Since

TABLE 1

OBSERVATIONS

ID	z_{em}	Date (UT)	Exposure (s)
0055−269.....	3.66	1991 May 13	2688
0114−089.....	3.16	1991 Aug 16	2688
0130−403.....	3.03	1991 May 13	2492
0143−016.....	3.14	1991 Jul 20	2688
0143−010.....	3.16	1991 Aug 16	2688
0324−408.....	3.06	1991 Mar 19	2690
0642+449.....	3.41	1991 Mar 18	2533
1402+045.....	3.20	1991 Jul 14	2688
1442+102.....	3.53	1991 Mar 19	2690
2126+159.....	3.26	1991 May 14	1602
2204+409.....	3.17	1990 Nov 23	2690
2359+068.....	3.23	1991 Jul 13	2688

the reduction of our slitless prism spectra is complicated by the *HST* spherical aberration, the processing and calibration of the data is described in some detail in § 2. The flux and wavelength calibrated extracted spectra are presented and commented upon individually in § 3. In § 4 we discuss the significance of our observations in light of our current understanding of intrinsic quasar spectra and the statistics of the Lyman continuum opacity problem. Our main results and conclusions are summarized in § 5.

2. OBSERVATIONS AND DATA REDUCTIONS

The 12 high-redshift quasars observed and the dates of observation are listed in Table 1. All observations were made with the f/96 camera of the FOC and the far-UV objective prism (PRISM1). The nominal 512 × 512 pixel detector format was used. The pixel size and field of view of this format are 22.36 ± 0.05 milliarcseconds (mas) and 11″.4, respectively (see Paresce 1992 for details of the FOC and its operating modes). Blind pointing target acquisition was used in all exposures. However, care was taken to remeasure the often inaccurate catalog positions of the targets beforehand on the *HST* system using the Guide Star Astrometric System (GASP) survey plates. The *HST* pointing was also deliberately offset by −7″.6 along the FOC detector *Y*-direction in order to compensate for the deflection of the far-UV objective prism and center the ≃250 pixel (5″.6) long dispersed images on the detector. Typical absolute pointing accuracies achieved in this manner were ≃1″–2″.

Because the FOC far-UV objective prism transmits light at all wavelengths above the MgF_2 cutoff at ≃λ1150, the diffuse background in images taken in this mode is dominated by geocoronal Lyα emission and zodiacal and scattered continuum light. Since the intensity of the diffuse Lyα component is highly variable with orbital position, three separate 900 s exposures were then taken of each target. These exposures were reduced individually and then co-added in order to maximize the S/N ratio of the final extracted spectra. The variations among the actual total exposure times listed in Table 1 reflect partly trimming due to the scheduling system, and partly interruptions in exposures caused by Solar Array disturbances.

A key characteristic of the FOC far-UV objective prism is its highly wavelength-dependent dispersion. The measured ultraviolet dispersion curve of the FOC f/96 prism and its derivative, giving the projected bandpass per pixel, is shown in Figures 1*a* and 1*b*. The dispersion decreases very rapidly with increasing wavelength, being equivalent to $\Delta\lambda \simeq 2$ Å per pixel at λ1200, and $\Delta\lambda \simeq 50$ Å per pixel at λ2500. This rapid increase in projected bandpass—which merely reflects the wavelength dependence of the index of refraction of MgF_2—continues into the visible reaching $\Delta\lambda \simeq 1000$ Å per pixel at the longest wavelengths near the $\lambda \approx 6500$ Å red sensitivity cutoff of the FOC detector. Because of this highly nonuniform dispersion, FOC far-UV objective prism spectra exhibit a very large dynamic range in terms of photon flux per pixel and are often saturated at their compressed red ends due to the count rate limitations of the photon counting FOC detectors. The well-defined red maxima in the dispersed images are nontheless also useful in that they provide an accurate fiducial point for determining the zero point of the wavelength calibration of the slitless two-dimensional spectra.

As described in detail by Greenfield et al. (1991), the aberrated *HST* point spread function as seen by the FOC consists of a very sharp (≃70 mas FWHM) central image core surrounded by a large (≃5″ diameter), but 10^{-2}–10^{-4} times fainter aberration halo. Since the length of the dispersed prism spectrum is comparable in size to the aberration halo radius, the spherical aberration of the *HST* telescope adversely affects the performance of the slitless FOC prisms in a manner that is compounded by their uneven dispersions. In particular, as can

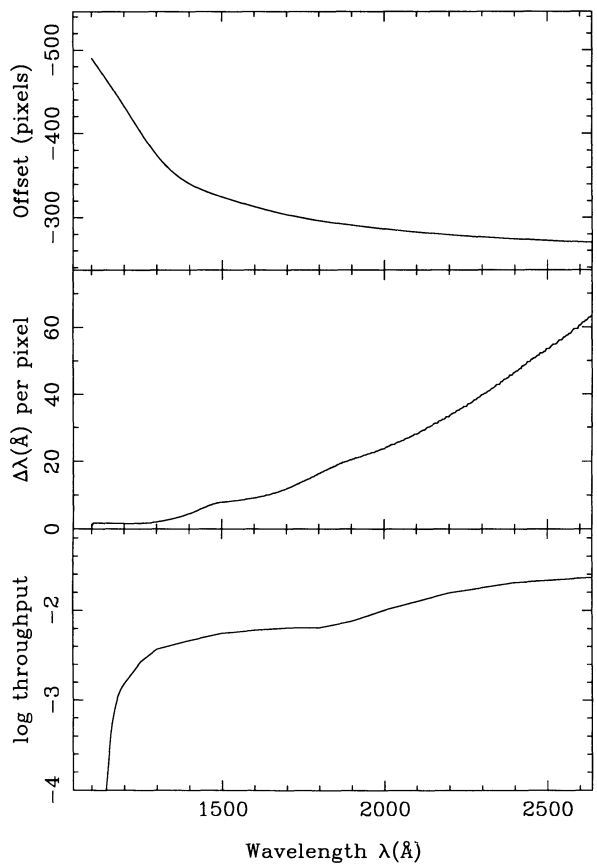

FIG. 1.—Calibration curves for the FOC f/96 far-UV objective prism (PRISM1). Panel (*a*) gives the dispersion curve in form of the deflection in detector pixels as a function of wavelength and panel (*b*) the corresponding projected bandpass per pixel. Panel (*c*) shows the effective throughput of the *HST* and FOC/PRISM1 combination for the specific extraction technique described in the text. The total throughput including the aberrated light is ≈5 times higher. The abrupt short-wavelength cutoff at λ1150 is caused by the MgF_2 substrate of the prism and the *HST* and FOC optical coatings.

be seen from the two examples of FOC far-UV prism exposures shown in Figures 2 and 5 (below), the portion of the dispersed images of interest covering the near- and far-UV are partly superposed on the aberration halo of the highly compressed red end of the spectrum. This wide-bandpass aberration halo acts as an additional source of background noise that leads to a further loss in sensitivity beyond the generic factor $\simeq 6$ loss caused by the spherical aberration in the case of isolated point sources (Burrows et al. 1991; Jakobsen Greenfield, & Jedrzejewski 1992). Nonetheless, because the *HST* point spread function (PSF) has such a sharp core, it is still possible to extract useful, albeit crude, low-resolution ultraviolet spectra from FOC prism exposures of faint obects and reach a limiting sensitivity that is fully competitive with that of the two grating spectrographs currently onboard *HST*.

2.1. *Extraction and Reduction of the Spectra*

All calibration and science exposures were reduced in the same manner, and utilized standard "pipeline" processed large-scale flat-fielded and geometrically corrected images. Our adopted approach for extracting one-dimensional spectra from the dispersed images attempts to optimize the spectral resolution and purity of the extracted spectra by utilizing only the $\simeq 20\%$ of the total light contained in the dispersed image of the central core of the PSF and treating the signal in the underlying aberration halo as "background". The method also permits a rather rigorous estimate of the statistical error of the final spectrum to be made. This latter point is crucial given that the target objects are very faint.

In order to maximize the throughput and S/N ratio at the shortest wavelengths of interest, the 12 $z_{em} \gtrsim 3$ quasars were observed using the bare far-UV prism; i.e., no additional filters were used. Hence the maxima at the red end of the spectra are extremely intense and sharp and resemble broad-band images of point sources. The corresponding spherical aberration halos affect the dispersed UV spectra down to about $\lambda 1450$ (cf. Fig. 5 below). In order to remove this dominant source of background in the ultraviolet portions of the dispersed images, the first step in the reduction involved locating the red peak in the image and subtracting the long wavelength aberration halo. This was achieved by least-squares fitting a representative PSF to the outer portions of the halo excluding areas closer than 20 pixels from the peak of the dispersed image. Since the compressed maxima of the FOC far-UV prism exposures span an extremely wide ($\Delta\lambda \simeq 3000$ Å) bandpass that does not correspond to any FOC filter, the template PSF used in the fitting and subtraction process was bootstrapped from the combined observation set by median filtering the normalized images of the 10 quasars observed that show no obvious ultraviolet flux in their spectra (see below). However, since the quasars observed do not have identical spectral slopes, low-level residual structure could in some cases be seen in the PSF subtracted images due to color mismatches between the average PSF template used and the actual image (the effects of variations in pointing jitter are negligible). Nonetheless, satisfactory removal of the bulk of the aberration halo of the visible end of the spectra was achieved in all cases, leaving the more uniform near and far-UV portions of the dispersed images.

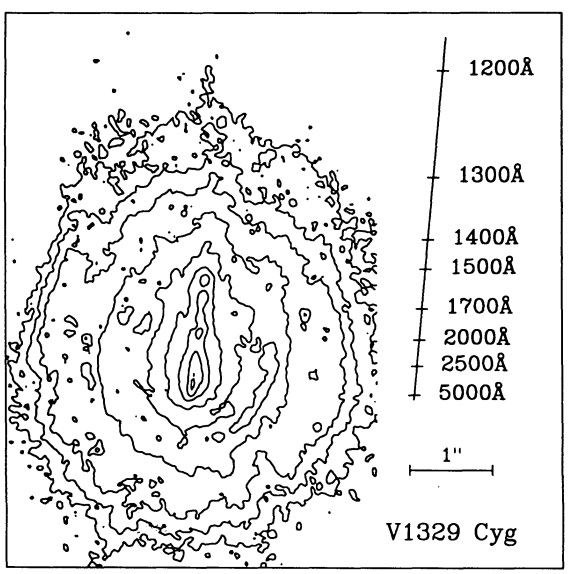

FIG. 2.—FOC far-UV objective prism calibration exposure of the symbiotic star V1329 Cyg showing the dispersed image core superposed on the aberration halo of the sharp red edge of the spectrum. This particular exposure was taken with the F195W filter also inserted in order to suppress the intensity of the red peak. The intensity contours are logarithmic and correspond to a factor 2 difference in surface brightness.

One-dimensional spectra representing the raw signal plus background counts contained in each detector wavelength bin were then extracted from the halo subtracted images by summing the total pixel counts in each image row contained within a 21 pixel wide (0.″47) window centered on the nominal location of the peak of the spectrum (taking into account the 6° tilt of the prism dispersion direction with respect to the image vertical). Two adjacent 21 pixel wide "background" spectra were then extracted on each side of the spectrum, averaged and subtracted from the raw peak spectrum. Since the shape of the aberration halo (whose diameter spans ~ 200 pixels) changes only slowly on scales comparable to the width of the extracted spectra, this step of the reduction corrects not only for the sky and detector background of the image, but also removes most of the underlying "low resolution" signal due to the dispersed images of the aberration halo in the near and far-UV.

The resulting extracted, 512 element long, raw spectrum consists mainly of the background-subtracted target counts contained in the dispersed image of the central $\approx 0.''1$ image core summed over each row of the FOC image (Fig. 3). In carrying out the summation over the pixel counts in each row, the technique of weighting with the profile of the FOC PSF was used in order to optimize the S/N ratio in the background limited far-UV portion of the spectrum (Robertson 1986). The resulting weighted spectra were renormalized to true FOC counts by scaling to the total counts contained in an identical raw spectrum extracted without pixel weighting.

The zero points needed for wavelength calibration were determined individually on the basis of the positions of the red maxima in the raw images. The extracted count spectra were resampled to a linear wavelength scale in a photon-conserving manner and then converted to absolute flux by division with the appropriate sensitivity factor and projected bandpass of each pixel. The 1 σ statistical error of each pixel in the resulting calibrated spectra were calculated by propagating the photon statistics of the original images through all steps of the extraction process. In particular, care was taken to include the statistical uncertainties associated with the PSF and background subtraction in the total error. The sub-exposures of each target were reduced individually and then co-added in an optimal manner by weighting with the pixel variance.

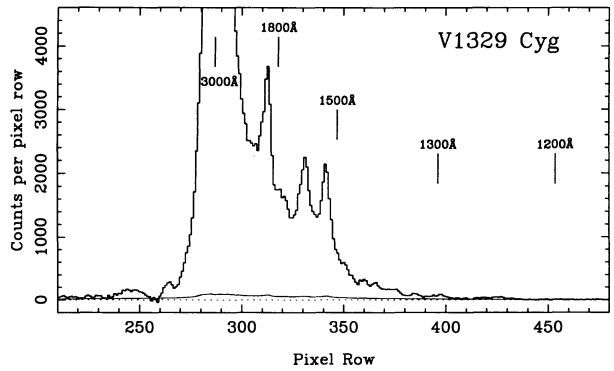

FIG. 3.—Raw one-dimensional spectrum of the symbiotic star V1329 Cyg extracted from the image shown in Fig. 2. The extraction procedure described in the text was used, except that no PSF subtraction was applied since the image was filtered. The detected emission lines are C III] λ1909, He II λ1640, and C IV λ1549, respectively. The lower curve gives the 1 σ photon statistical uncertainty.

2.2. *On Orbit Calibration Verification*

The calibration of the FOC far-UV prism and our adopted methods of reduction were validated in orbit based on observations of suitable wavelength and photometric standards.

The pre-launch dispersion curve of the FOC far-UV objective prism was checked against observations of the symbiotic star V1329 Cyg (Fig. 2). The raw and calibrated far-UV prism spectra of this object are shown in Figures 3 and 4, respectively. Based on the good agreement between the positions of the observed and predicted emission lines in the spectra, we estimate that our wavelength calibration should be accurate to ~10–20 Å in the $\lambda < 2000$ Å wavelength range of interest.

The photometric calibration of the FOC f/96 far-UV prism was derived from observations of the UV standard stars HZ4 and BPM 16274 (Bohlin et al. 1990) and the low-redshift quasar PKS 1202+281 (Kinney et al. 1991; see Fig. 5). The raw FOC spectra of these objects were extracted in the manner outlined above, and the conversion factor between FOC counts and absolute flux as a function of wavelength was derived from comparison with the absolute calibrated *IUE* spectra of the same objects. The resulting photometric calibration curve (Fig. 1*c*) mimics closely the nominal FOC response curve in shape, but reflects the fact that only ~20% of the total light entering the instrument is contained in the image core and collected by the adopted extraction technique. A comparison between the calibrated FOC and *IUE* observations of PKS 1202+281 is shown in Figure 6. However, since PKS 1202+281 is known to be variable (Kinney et al. 1991), our absolute far-UV flux calibration may only be accurate to within a factor of ~2 at the shortest wavelengths.

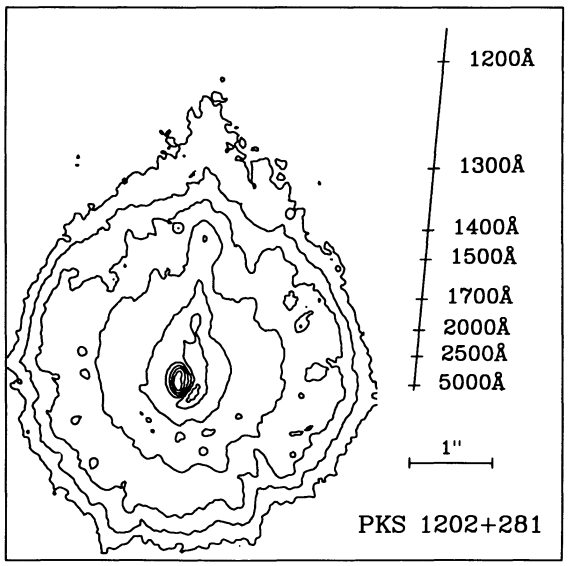

FIG. 5.—FOC far-UV objective prism calibration exposure of the $z_{em} = 0.165$, $V = 15.6$ quasar PKS 1202+281. The red peak of the spectrum is saturated in this unfiltered exposure. The Lyα emission line can be seen near λ1400. The intensity contours are logarithmic and correspond to a factor 2 difference in surface brightness.

3. RESULTS

Illustrative examples of extracted raw prism spectra of two of the 12 target quasars listed in Table 1 are shown in Figure 7. The FOC prism spectra are photometrically unreliable at wavelengths $\lambda \gtrsim 1800$ Å because of the effects of detector saturation and subtraction of the aberration halo. However, below

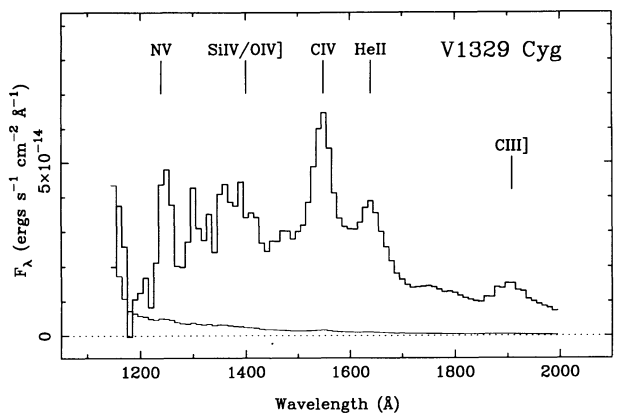

FIG. 4.—Wavelength and flux calibrated spectrum of V1329 Cyg derived from the raw extracted spectrum shown in Fig. 3. The lower curve gives the 1 σ photometric uncertainty per 10 Å wavelength bin due to the photon statistics. Note the good accuracy of the wavelength calibration and the decrease in spectral resolution at the longer wavelengths.

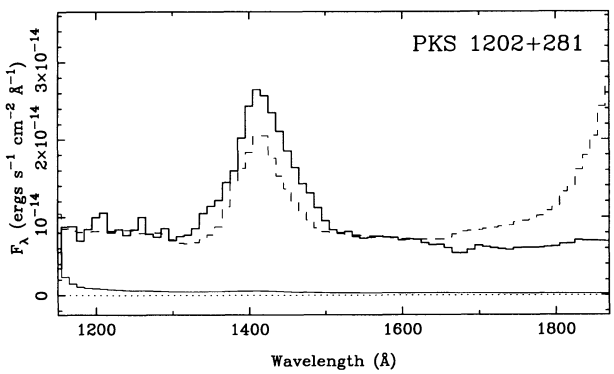

FIG. 6.—Wavelength and flux calibrated far-UV spectrum of the Lyα region of PKS 1202+281 derived from the raw extracted spectrum shown in Fig. 5. The lower curve gives the 1 σ photometric uncertainty per 10 Å wavelength bin due to the photon statistics. The dashed curve shows the anticipated spectrum obtained by adjusting the observed *IUE* spectrum of this object to the spectral resolution of FOC far-UV prism. The discrepancy at wavelengths above $\lambda \simeq 1800$ Å is an artifact of detector saturation and the adopted PSF subtraction technique.

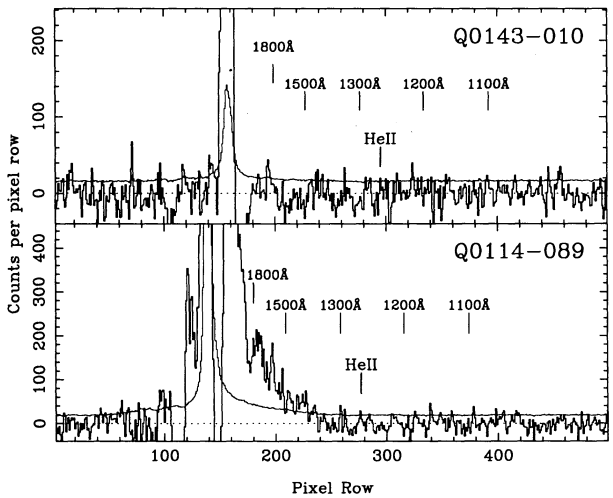

FIG. 7.—Examples of raw extracted spectra for two representative $z_{em} > 3$ quasars. The thin curves give the 1 σ photon statistical uncertainties per pixel row. The dips in the counts seen longward of λ1800 are artifacts of the PSF subtraction technique and the extracted spectra are unreliable above this wavelength. Whereas Q0114−089 shows a significant far-UV signal down to $\simeq\lambda$1400, Q0143−010 is not detected at any wavelength shortward of λ1800. The anticipated position of the He II λ304 line is also marked.

this limit, the data are photometrically and statistically well-behaved. In the case of Q0143−010 where no far-UV flux is detected at all, the extracted background corrected counts fluctuate around zero in a manner fully consistent with the estimated statistical error. Conversely, Q0114−089 is one of only two of the 12 quasars observed in which a far-UV flux is detected. Both the raw image and extracted spectrum of this object show clear evidence for a statistically significant flux down to $\lambda \simeq 1350$ Å in wavelength.

The flux and wavelength calibrated spectra of all 12 objects observed and the corresponding 1 σ flux uncertainties per 10 Å wide wavelength bin are plotted in Figure 8. The limiting sensitivity of our observations varies somewhat with target due to variations in the image background and net exposure time, but lies in the range $F_\lambda \simeq 2\text{–}4 \times 10^{-16}$ ergs s^{-1} cm^{-2} Å^{-1} (3 σ). Also shown in Figure 8 are the positions of the emitted He II λ304 line in each object and the 3 σ upper limits on the average continuum flux measured within a $\Delta\lambda = 50$ Å wide wavelength band located just-longward of the He II line. The latter flux limits are also listed in Table 2.

For reference, we also show as dashed lines in Figure 8 estimates of the anticipated far-UV spectrum of each quasar in the hypothetical case of no intergalactic Lyman continuum absorption. These spectra were calculated through naive

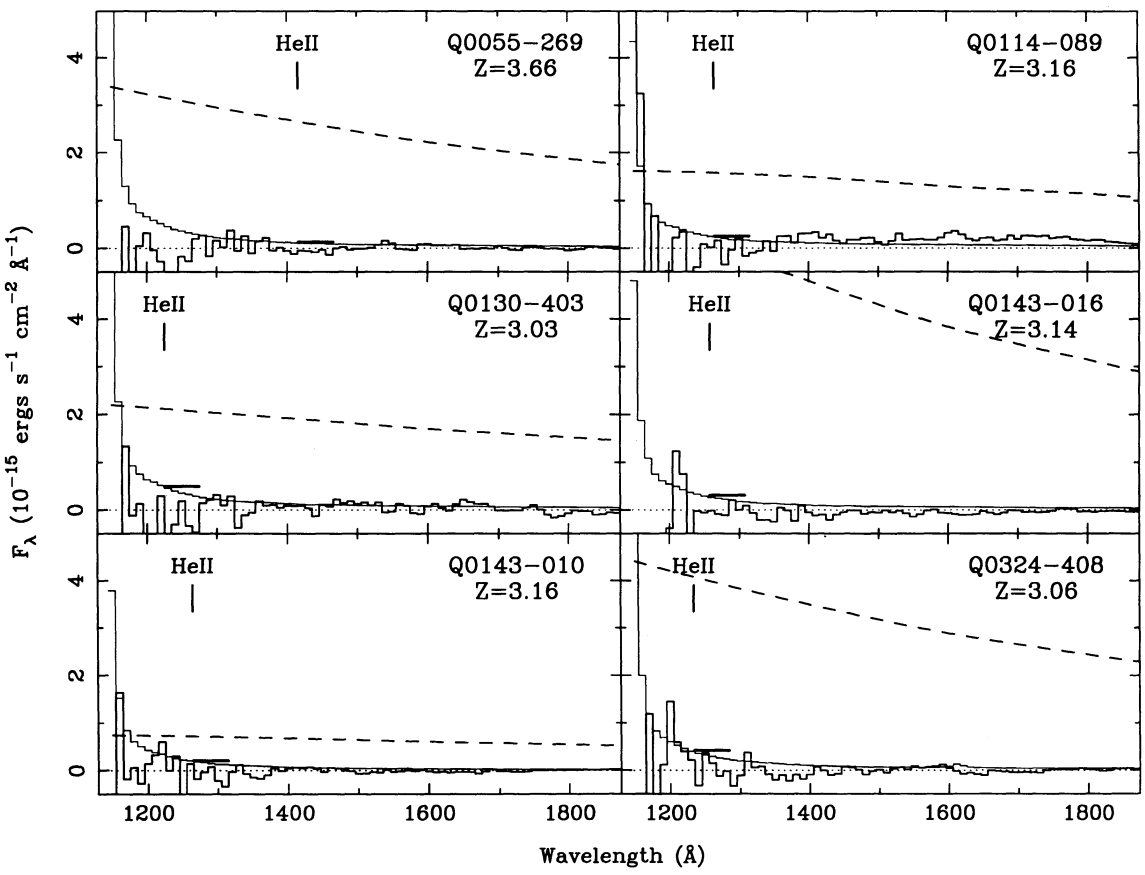

FIG. 8*a*

FIG. 8.—Mosaic of the calibrated FOC far-UV prism spectra of the 12 $z_{em} \gtrsim 3$ quasars observed. The thin curve gives the 1 σ photometric uncertainty per 10 Å wavelength bin due to the photon statistics. The anticipated positions of the He II λ304 transition, and the 3 σ upper limits on the average fluxes within a $\Delta\lambda = 50$ Å wavelength bin just longward of the He II line are also marked. The dashed curves are an estimate of the anticipated flux in the case of no intergalactic Lyman continuum absorption obtained by extrapolating the optical power-law spectra and reddening with a standard UV interstellar extinction law (see text).

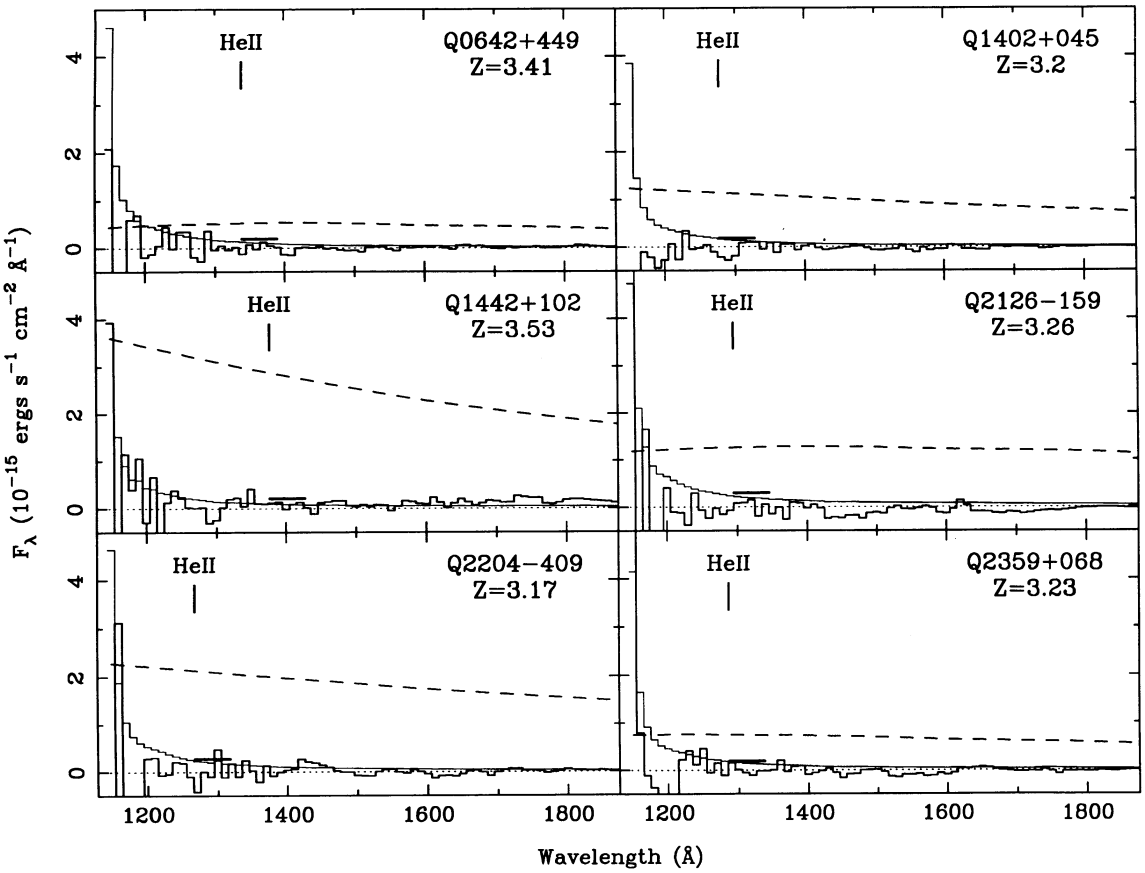

FIG. 8*b*

extrapolation of the $F_\nu \propto \nu^\alpha$ power-law continuum seen in the visible, but taking interstellar extinction into account (see § 4).

Our main result is that only two of the 12 high-redshift quasars observed—namely Q0114−089 (UM 670) and Q1442+102 (OQ 172)—are detected at all at far-UV wavelengths below λ1800. In both cases, however, the detected flux appears to decrease at the shortest wavelengths, and neither object shows a statistically significant flux at the wavelength of the redshifted He II λ304 line.

The implication of this null result for models of the intrinsic extreme ultraviolet spectra of quasars and the intervening hydrogen continuum opacity is discussed further in § 4. Brief comments on the 12 objects observed with an emphasis on what is known about their lines of sight from the appearance of the optical absorption spectra, follow.

TABLE 2

FLUX AND ABSORPTION PARAMETERS

ID	V	α	E_{B-V}	F_λ[a]	$q_{3\sigma}$	p_0	p_B
Q0055−269.....	17.9	0.47	0.032	1.30	0.049	7.8%	18.4%
Q0114−089.....	17.9	0.75	0.074	2.54	0.161	7.9	13.0
Q0130−403.....	17.5	1.00	0.028	4.96	0.234	7.2	7.6
Q0143−016.....	17.6	0.18	0.051	3.11	0.056	14.2	20.4
Q0143−010.....	18.5	1.00	0.051	2.10	0.292	4.4	2.3
Q0324−408.....	17.6	0.50	0.027	4.17	0.102	11.2	5.4
Q0642−449.....	18.5	0.64	0.200	1.92	0.365	1.8	0.3
Q1402+045.....	18.5	0.74	0.037	1.79	0.158	7.4	3.3
Q1442+102.....	18.0	0.38	0.030	2.13	0.074	7.3	15.7
Q2126−159.....	17.0	1.43	0.085	2.97	0.237	4.7	3.7
Q2204−409.....	17.5	1.00	0.023	2.85	0.134	8.0	12.1
Q2359+068.....	18.4	0.89	0.087	1.97	0.263	5.1	9.7

[a] 3 σ upper limit longward of emitted 304 Å in units of 10^{-16} ergs s^{-1} cm^{-2} Å^{-1}.

3.1. *Notes on Individual Objects*

3.1.1. *Q0055−269*

At a redshift of $z_{em} = 3.66$, Q0055−269 is the most remote of the 12 quasars observed. The object is one of only a handful of quasars included in the survey of Sargent et al. (1989) that do not contain a Lyman limit absorption system within the optical window ($z_{abs} \gtrsim 2.6$). Continuum absorption associated with the six metal line C IV systems detected in this object by Steidel (1990) between $z_{abs} \simeq 2.95$ and $z_{abs} \simeq 3.67$ cannot therefore explain the lack of far-UV flux in this object. However, Steidel (1990) also detected a Mg II doublet and two Fe II lines at $z_{abs} = 1.534$. It is highly likely that a Lyman limit absorber of density $N_{H\,I} \gtrsim 2 \times 10^{18}$ cm^{-2} associated with this system is responsible for attenuating the flux below $\lambda = 2311$ Å.

3.1.2. *Q0114−089 (UM 670)*

This $z_{em} = 3.16$ quasar is another example of an object included in the Sargent et al. (1989) survey that does not show any Lyman edges in its optical spectrum. The absorption line spectrum of Q0114−089 has been discussed by Sargent, Boksenberg, & Steidel (1988) and Khare, York, & Green (1989), who detected C IV systems at $z_{abs} = 2.299$, 2.539, and 3.105, respectively.

Q0114−089 is one of only two objects in which we detect a

far-UV continuum, albeit at a very faint level corresponding to an absolute flux of order $F_\lambda \simeq 2$–4×10^{-16} ergs s^{-1} cm^{-2} Å^{-1}. The reality of the far-UV signal is nevertheless obvious from the raw FOC image. An expanded view of the calibrated FOC far-UV prism spectra of Q0114−089 is shown in Figure 9. Since the S/N ratio is rather low ($\lesssim 4$ per wavelength bin), we do not attach much significance to the apparent spectral features present in the spectrum, except for the clear drop in flux seen below $\lambda \simeq 1360$ Å. If due to a Lyman edge, the inferred redshift of the absorber is $z_{abs} \simeq 0.5$. The intermediate resolution spectrum published by Sargent, Steidel, & Boksenberg (1989) reveals no obvious Mg II doublet near this redshift, but such a line could easily be lost in the Lyman forest.

The significance of our detection of this object at a rest wavelength corresponding to $\lambda \simeq 330$ Å is discussed in § 4.

3.1.3. *Q*0130−403

The absorption line spectrum of this $z_{em} = 3.03$ quasar has been studied by Whelan, Smith, & Carswell (1979), who reported the presence of a complex C IV system at $z_{abs} = 2.56$. The blue continuum of Q0130−403 was observed by Osmer (1979) and Smith et al. (1981). An optically thin Lyman edge ($N_{H\,I} \approx 2 \times 10^{17}$ cm^{-2}) is present at $z_{abs} \simeq 2.85$, but the object is otherwise detectable down to the atmospheric cutoff. Since the Lyα absorption at $z_{abs} = 2.56$ is not particularly strong, we consider is unlikely that this complex is responsible for absorbing the far-UV flux.

3.1.4. *Q*0143−016 (*UM* 366; *PHL* 7750)

This $z_{em} = 3.14$ quasar has been observed by Smith et al. (1981) and Sargent et al. (1989). The latter authors report the presence of metal line systems at $z_{abs} = 1.038$, 1.285, 1.579, and 1.613. Although Q0143−016 is detectable down to the atmospheric cutoff and has an unusually energetic optical spectrum ($\alpha \simeq 0.18$), Lyman continuum absorption associated with one or more of these systems could be responsible for quenching its far-UV flux.

3.1.5. *Q*0143−010, (*UM* 368)

The optical spectrum of this $z_{em} = 3.16$ quasar is known to contain a Lyman limit system at $z_{abs} = 2.82$ (Smith et al. 1981; Oke & Korycansky 1982). Since the object is also rather faint ($V \simeq 18.5$), it is possible that absorption in this system alone can account for our nondetection in the UV.

3.1.6. *Q*0324−408

Q0324−408 ($z_{em} = 3.06$) is the only broad absorption line (BAL) quasar contained in our sample. The complex optical absorption spectrum of this object has been studied by Whelan et al. (1979) and Smith et al. (1981). As is common in BAL objects, the two broad trough systems seen at $z_{abs} \sim 2.82$ and $z_{abs} \sim 2.89$ appear to be of extremely high ionization judging from the absorption seen in C IV, N V, and O VI. However, Osmer (1979) and Smith et al. (1981) also detect a Lyman edge near $z_{abs} \sim 2.9$, which could be associated with the latter trough system. Since the corresponding Lyα line falls in the N V trough of the $z_{abs} \simeq 2.82$ absorption system, it is difficult to say whether this Lyman edge is responsible for absorbing the UV flux.

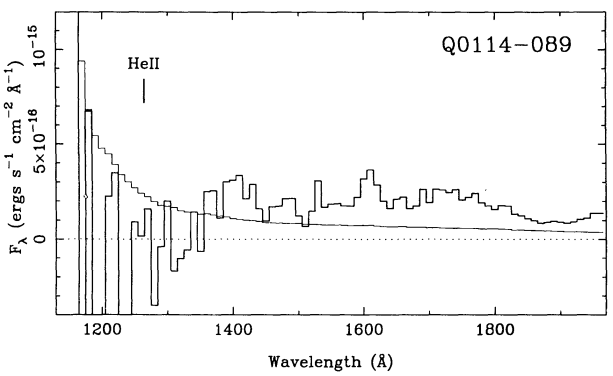

FIG. 9.—Detailed plot of the observed spectrum of Q0114−089, one of two objects detected in the far-UV.

3.1.7. *Q*0642+449 (*OH* 471)

The absorption line spectrum of this well-known $z_{em} = 3.41$ quasar has been discussed by Carswell et al. (1975), Oke & Korycansky (1982), Antonucci, Kinney, & Ford (1989), Khare, York, & Green (1989), and Sargent et al. (1989). The object displays at least three C IV metal line systems at $z_{abs} = 2.972$, 3.124, and 3.248. Two presumably related Lyman edges at $z_{abs} \simeq 3.12$ and $z_{abs} \simeq 3.29$ conspire to absorb the optical blue continuum shortward of λ3800. Although these two systems are not necessarily completely optically thick at far-UV wavelengths, a low redshift Mg II/Fe II system is also present at $z_{abs} = 1.246$. Neutral hydrogen absorption from the latter system will absorb the spectrum below λ2050. The interstellar extinction in the direction of this object is rather high.

3.1.8. *Q*1402+045 (*PKS*)

The spectrum of this $z_{em} = 3.20$ object has been studied by Peterson et al. (1979), Oke & Koyrcansky (1982), and more recently by Wolf et al. (1986) and Antonucci et al. (1989). In addition to a Lyman continuum edge at $z_{abs} \sim 3.1$, the object also displays three candidate damped Lyα systems at the slightly lower redshifts $z_{abs} \simeq 2.71$, 2.69, and 2.48 (Turnshek et al. 1989). Our nondetection of this object could be due to one or more of these systems.

3.1.9. *Q*1442+102 (*OQ* 172, *MC* 2)

This classical high-redshift quasar has been studied by a number of authors, most recently by Sargent, Boksenberg, & Steidel (1988), Morton et al. (1989), Antonucci et al. (1989), and Barthel, Tytler, & Thompson (1990). Q1442+102 is a rather unique object in that in spite of its large redshift ($z_{em} = 3.53$) its line of sight appears to be unusually clear. The blue continuum of Q1442+102 is detectable down to the atmospheric cutoff and reveals no signs of any Lyman continuum edges within the optical window. Moreover, only two reasonably firm C IV metal line systems at $z_{abs} = 2.563$ and $z_{abs} = 2.634$ have been identified in the spectrum. Q1442+102 has therefore a long-standing history as a prime candidate for far-UV observations with *HST*.

Remarkably, Q1442+102 is the second object in which we detect a far-UV signal, the reality of which is clear from the raw data. The calibrated FOC objective prism spectrum of Q1442+102 is shown in detail in Figure 10. Although very faint, the object clearly displays a statistically significant flux at the $F_\lambda \simeq 2 \times 10^{-16}$ ergs s^{-1} cm^{-2} Å^{-1} level down to at least $\lambda \simeq 1550$ Å. Below this wavelength, however, we are extremely reluctant to claim a positive detection given that the net signal is at the very limit of the sensitivity and credibility of our data. In particular, we consider the apparent emission feature near λ1350 to be almost certainly spurious.

Q1442+102 has also been observed with the Faint Object Spectrograph onboard *HST* by Beaver et al. (1992), who

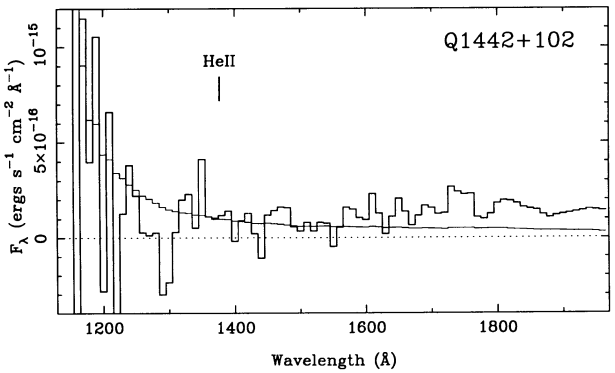

FIG. 10.—Detailed plot of the observed spectrum of Q1442+102, one of two objects detected in the far-UV.

detected a drop in the spectrum at $\lambda \simeq 1550$ Å. Unfortunately, the (red channel) FOS spectrum of Q1442+102 does not extend to shorter wavelengths. In the region of overlap the FOC and FOS absolute far-UV fluxes of Q1442+102 agree to better than a factor of ~ 2, thereby adding confidence to our absolute flux calibration.

The significance of our detection of Q1442+102 down to $\lambda \simeq 345$ Å rest wavelength is discussed in § 4.

3.1.10. *Q2126−159 (PKS)*

The rich absorption spectrum of this well-studied bright high-redshift quasar ($V \simeq 17.1$, $z_{em} = 3.261$) has most recently been discussed by Sargent et al. (1988), Sargent, Steidel, & Boksenberg (1989), and Khare et al. (1989). In addition to a number of C IV systems seen in the spectrum in the range $z_{abs} = 2.02$–2.97, two Lyman limit edges are also detected just above the atmospheric cutoff at $z_{abs} = 2.792$ and $z_{abs} = 2.973$. It is possible that the former system has a sufficiently high neutral hydrogen column density ($N_{H\,I} \gtrsim 3 \times 10^{18}$ cm^{-2}) to be optically thick at far-UV wavelengths.

3.1.11. *Q2204−409*

Q2204−409 ($z_{em} = 3.17$) is another prime candidate for far-UV observations in that the object is relatively bright ($V \simeq 17.5$) and detectable down to the atmospheric cutoff at $z_{abs} \gtrsim 2.6$ (Osmer 1979; Smith et al. 1981; Wilkes 1984). In fact, an attempt to observe this object in the far-UV with *IUE* has been made previously by Wilson, Carnochan, & Gondhalekar (1979), who claimed a positive detection down to $\lambda \simeq 1200$ Å. The absolute far-UV fluxes reported by Wilson et al. lie in the range $F_\lambda \simeq 4$–19×10^{-16} ergs s^{-1} cm^{-2} Å^{-1}.

As is clear from Figure 8, however, the detection reported by Wilson et al. is not confirmed by our FOC objective prism observations of Q2204−409. The FOC observations instead imply that this object is fainter than $F_\lambda \lesssim 3 \times 10^{-16}$ ergs s^{-1} cm^{-2} Å^{-1} throughout the far-UV at a high level of confidence.

The line of sight to Q2204−409 is known to intercept two metal line absorption systems at redshifts below $z_{abs} \simeq 2.7$; a C IV system at $z_{abs} = 2.628$ and an Al III doublet at $z_{abs} = 1.845$ (Willinger et al. 1989; Steidel 1990). We consider it highly likely that the latter system has a column density $N_{H\,I} \gtrsim 1 \times 10^{18}$ cm^{-2} and is therefore responsible for absorbing the spectrum completely throughout the UV at wavelengths $\lambda \lesssim 2600$ Å.

3.1.12. *Q2359+068*

This $z_{em} = 3.23$ quasar from the Sargent et al. (1989) survey is noteworthy in that it does not contain any Lyman limit systems within the optical window in spite of showing 7 C IV systems at $z_{abs} \gtrsim 2.7$. A lower redshift Mg II system is also seen at $z_{abs} = 0.8958$. This system can, however, only explain our lack of detection at wavelengths below $\lambda = 1730$ Å. Presumably, the line of sight to this object intercepts a dense absorber somewhere in the $1.5 \lesssim z_{abs} \lesssim 2.7$ redshift range not probed by the Lyman limit and Mg II observations.

4. DISCUSSION

The primary motivation for the observations described in this paper is the hope of identifying one or more only modestly absorbed quasars at $z_{em} > 3$ bright enough in the far-UV to permit the detection and study of intergalactic He II λ304 in absorption. Although we have not yet succeeded in this goal, it is of interest to analyze the significance of our results for future searches for UV-bright quasars at high redshift.

The apparent brightness of high redshift quasars at extreme ultraviolet wavelengths is obviously determined by two main factors: the intrinsic emission spectrum of quasars at these energies, and the strength of the intervening Lyman continuum absorption. The first factor has a bearing on models for quasar continuum emission, whereas the second is relevant for the topic of quasar absorption lines and the question of the overall transparency of the universe in the extreme and far-UV.

Quasars are widely believed to be powered by mass accretion onto massive ($M \approx 10^7$–10^9 $M_\odot$) black holes. In this model thermal emission from the accretion disk surrounding the central massive object gives rise to a "big blue bump" in the spectrum that dominates the emission at far and extreme ultraviolet rest energies (e.g., Edelson & Malkan 1986). In the simplest "thin accretion disk" versions of this model, the thermal emission is emitted at the Eddington limit from a region comparable in size to the Schwarzschild radius of the black hole. Consequently, relatively cool ($T \simeq 3 \times 10^4$ K) accretion disks are predicted, and the associated thermal emission is therefore expected to peak at round $\lambda \simeq 900$ Å emitted wavelength (cf. Laor & Netzer 1989). Although there is good evidence that a blue bump feature is present in the spectra of many quasars, recent observations of luminous quasars in the far-UV (Reimers et al. 1989, 1992) and in soft X-rays (Elvis et al. 1991; Bechtold et al. 1987a) strongly suggest that the intrinsic spectrum peaks at much shorter extreme-UV wavelengths, and that the thermal emission therefore is considerably hotter than predicted in the thin accretion disk model. This has been interpreted to imply that the accretion process is highly anisotropic and "super Eddington" in nature and that the bulk of the thermal emission comes from a very small area in the accretion disk (Bechtold et al. 1987a; Madau 1988; Courvoisier & Clavel 1991). In any event, the prospects of using high-redshift quasars as background sources for observing intergalactic helium absorption are obviously better for sources with intrinsically energetic extreme-UV spectra.

The second factor affecting the apparent far-UV fluxes of high redshift quasars is perhaps better understood at present. As discussed in detail by Møller & Jakobsen (1990), the line of sight frequency, column density spectrum, and redshift evolution of the various classes of neutral hydrogen bearing quasar absorption-line systems are sufficiently well-known that the statistics of the highly stochastic cumulative absorption process can be predicted with reasonable accuracy through Monte Carlo simulations. In particular, the probability of encountering a given total opacity at a given received far-UV wavelength out to a given redshift can be calculated at least to

within an order of magnitude. Such probability calculations can be used to gauge the statistical likelihood of obtaining our preliminary null result by chance, given the absolute sensitivity of our survey and a model for the intrinsic extreme-UV emission of quasars.

In view of the uncertainties mentioned above, we have in the following adopted the simple hypothesis that luminous quasars emit in the extreme-ultraviolet in accordance with a simple extrapolation of their $F_\nu \propto \nu^{-\alpha}$ optical spectra, as normalized to their visible magnitudes. The V-magnitudes and spectral indexes adopted for our targets are listed in Table 2, and were (in order of preference) taken from data in Sargent et al. (1989), Oke & Korycansky (1982), Osmer (1979), and Smith et al. (1981). The average spectral index of our sample is $\bar{\alpha} = 0.75$, which is typical of quasars as a class.

Since interstellar extinction can be important at the short far-UV wavelengths of interest ($A_\lambda/E_{B-V} \simeq 9$–10), we have taken galactic interstellar extinction into account in calculating the assumed unabsorbed apparent fluxes of our targets. The adopted E_{B-V} values listed in Table 2 were estimated from the integrated 21 cm column densities of Stark et al. (1989). A standard gas-to-dust ratio and UV extinction curve (Savage & Mathis 1979) were assumed. For a few of our targets, the interstellar extinction amounts to an attenuation of the received far-UV flux by as much as a factor $\simeq$2–3.

In Table 2 we list the inferred upper limit on the intergalactic transmission out to each target, $q_{3\,\sigma}$, defined by the ratio between the listed upper limit on the observed far-UV flux at redshifted He II λ304, F_λ, and the corresponding extrapolated unabsorbed flux. In the second to last column in Table 2 we give the corresponding probability, p_0, of encountering a transmission greater or equal to $q_{3\,\sigma}$ for a random line of sight out to the redshift of the target. These probabilities were derived through Monte Carlo simulations as described in Møller & Jakobsen (1990), and correspond closely to the transmission quantiles given in Figure 6 of that paper. It is seen that even with our relatively optimistic assumption concerning the intrinsic emission of our targets in the extreme UV, the corresponding limits on the maximum transmission are relatively high and span the range $q_{3\,\sigma} \simeq 0.05$–0.37. Nonetheless, the probability of encountering less absorption than implied by these transparencies is typically only of order $p \simeq 5\%$–10%. The combined probability of our not detecting any of the 12 objects at redshifted He II λ304 can be estimated by multiplying the individual probabilities of encountering absorption *more* severe than $q_{3\,\sigma}$ for all targets: $P_0 \simeq \prod(1 - p_0) \simeq 40\%$.

In actual fact, the calculated probabilities quoted above are too conservative in the sense that they refer to *random* lines of sight, whereas most of our targets were selected on the basis of their optical spectra not displaying any obviously dense absorbers in the redshift window accessible from the ground. Hence our targets are necessarily biased toward sight lines that are largely devoid of large column density systems, at least at high redshift near the quasars. The last column in Table 2 lists the probability, p_B, of exceeding the $q_{3\,\sigma}$ when this bias is taken into account in the Monte Carlo simulations by excluding systems above a certain column density from falling in the optical window as judged from the available spectra in the literature (i.e., typically excluding systems with $N_{\rm H\,I} \gtrsim 2 \times 10^{17}$ cm^{-2} within $2.6 \leq z_{\rm abs} \leq z_{\rm em}$). In cases where Lyman limit systems are known to be present in the optical spectra, the optical depth of the system was bracketed and known column density spectrum of such systems was used to simulate the range of possible absorption due to the system at shorter wavelengths. In such cases, p_B is normally less than p_0 due to the presence of the Lyman limit system. On the other hand, in objects with optical spectra devoid of such systems, the probability of reaching a given transmission is typically 2–3 times higher than that of a corresponding random line of sight out to the same redshift.

With the biased-corrected probabilities, the combined likelihood of our nondetections decreases to $P_B \simeq \prod(1 - p_B) \simeq 30\%$. This rather large value of P_B implies that, given the current sensitivity of *HST* and the hurdle posed by the cumulative intervening neutral hydrogen absorption, we should not be surprised at not yet having succeeded in detecting a $z_{\rm em} > 3$ quasar at redshifted He II λ304 in only 12 attempts.[16]

The large inferred value of P_B also implies that our data are statistically consistent with the assumption made that luminous quasars emit in the extreme ultraviolet in accordance with an extrapolation of their $F_\nu \propto \nu^\alpha$ optical spectra. The derived value of P_B is not overly sensitive to the assumed intrinsic spectra. Arbitrarily halving and doubling the calculated intrinsic extreme UV fluxes with respect to the nominal extrapolated values lead to null result probabilities of $P_B \simeq 49\%$ and $P_B \simeq 18\%$, respectively. Only intrinsic flux levels as high as a factor $\gtrsim$4 above the optical extrapolation (corresponding to an average effective spectra index of $\bar{\alpha} \simeq -0.2$) are excluded by our data at any reasonable level of confidence ($1 - P_B \gtrsim 90\%$).

The above considerations only serve to place an upper limit on the extreme-UV emission of quasars. However, our two cases of detections at extreme UV rest wavelengths slightly longward of emitted He II λ304 provide positive evidence that at least some high-redshift quasars do emit in the Lyman continuum at levels comparable to the optical extrapolation. The apparent flux of Q0114−089 at $\lambda = 330$ Å rest wavelength is $F_\lambda \simeq 2.5 \times 10^{-16}$ ergs s^{-1} cm^{-2} Å^{-1}, and the flux of Q1442+102 at $\lambda = 345$ Å is $F_\lambda \simeq 1.5 \times 10^{-16}$ ergs s^{-1} cm^{-2} Å^{-1}. Even with no correction for Lyman continuum absorption, these fluxes imply apparent optical-to-UV effective spectral indices of $\alpha \lesssim$ 2–3 and color temperatures of $T \gtrsim 4 \times 10^4$ K for the intrinsic spectra.

The inferred transmissions toward Q0114−089 and Q1442+102 at the shortest detected wavelengths calculated from the extinction-corrected extrapolated optical spectra are $q \simeq 0.17$ and $q \simeq 0.06$, respectively. According to the Monte Carlo simulations, these values place Q0114−089 and Q1442+102 on the $p_B \simeq 12\%$ and $p_B \simeq 15\%$ probability quantiles. This is entirely consistent with the fact that the two detected objects represent two out of 12, or 17% of our sample. In other words, the intrinsic extreme-UV fluxes of Q0114−089 and Q1442+102 cannot be much fainter than the extrapolated fluxes, since unrealistically clear, and hence highly improbable, sight lines would otherwise be required in order to explain our positive detections.

The true absorption-corrected effective spectral indices of the intrinsic spectra of Q0114−089 and Q1442+102 are therefore most likely closer to $\alpha \simeq 0.6$. This implies that the peak (in νF_ν) of the "big blue bump" in the spectra of these two

[16] Note that, like Møller & Jakobsen (1990), we have ignored photoelectric absorption due to neutral helium below λ504 in our opacity calculations. For reasons outlined in the Appendix, the He I column density is expected to be significant only in systems that are already completely optically thick in H I. Adding a 10% He I column density to all absorbers having $N_{\rm H\,I} \geq 1 \times 10^{18}$ cm^{-2} changes the combined null probability only slightly to $P_0 \simeq 33\%$.

objects occurs at wavelengths below the shortest observed $\sim\lambda 330$. Our two positive detections are therefore in accord with previous far-UV observations that indicate that the extreme ultraviolet spectra of luminous quasars are considerably more energetic than predicted by the simplest accretion disk models (Bechtold et al. 1987a; Reimers et al. 1989; Beaver et al. 1991).

In summary, we conclude that the fact that we have only detected two out of 12 $z_{em} > 3$ quasars at extreme-UV rest wavelengths can mainly be attributed to intervening Lyman continuum absorption and not to luminous quasars being intrinsically faint at these energies.

5. SUMMARY AND CONCLUSIONS

We have presented the first FOC far-UV objective prism observations of high-redshift quasars. The primary aim of this ongoing survey is to identify one or more quasars at $z_{em} > 3$ that are not too severely absorbed in the far-UV due to cumulative intervening neutral hydrogen Lyman continuum absorption and bright enough to permit more detailed follow-up observations of redshifted intergalactic He II $\lambda 304$ absorption using the *HST* grating spectrographs.

In orbit calibration exposures have shown that the slitless FOC far-UV objective prism mode is capable of reaching a limiting continuum flux of $F_\lambda \simeq 2 \times 10^{-16}$ ergs s^{-1} cm^{-2} Å^{-1} at 1200 Å $\lesssim \lambda \lesssim$ 1800 Å. In spite of the complications and factor ≈ 6 loss in sensitivity introduced by the *HST* spherical aberration, this sensitivity is adequate for the task at hand, since it is well below the minimum flux for which lengthy and more detailed follow-up spectroscopic observations are feasible in practice with the present *HST* instrumentation.

We have presented prism observations of 12 quasars selected from the literature on the basis of their redshift ($3.0 \lesssim z_{em} \lesssim 3.7$), brightness ($V \lesssim 18.5$) and appearance of their optical absorption spectra. As anticipated beforehand, the far-UV spectra of the majority of these high redshift quasars are seriously affected by intervening Lyman continuum absorption. At our limiting sensitivity, all but two of the objects are not detected at all in the far-UV at wavelengths $\lambda \lesssim 1800$ Å. Q0114−089 (UM 670, $z_{em} = 3.16$) does show a faint flux of intensity $F_\lambda \simeq 2$–4×10^{-16} ergs s^{-1} cm^{-2} Å^{-1}, but only down to $\lambda \simeq 1360$ Å ($\lambda \gtrsim 330$ Å rest wavelength). Similarly, Q1442+102 (OQ 172, $z_{em} = 3.53$) is detected at the $F_\lambda \simeq 2 \times 10^{-16}$ ergs s^{-1} cm^{-2} Å^{-1} level, but most likely only above $\lambda \simeq 1550$ Å ($\lambda \simeq 345$ Å emitted wavelength). Presumably the lack of flux at shorter wavelengths in these two objects is caused by intervening Lyman limit systems located at $z_{abs} \simeq 0.5$ and $z_{abs} \simeq 0.7$, respectively. Future FOC prism observations of Q1442+102 and Q0114−089 at the factor ≈ 4 increased sensitivity anticipated with COSTAR will clearly be highly worthwhile.

Although none of our targets is reliably detected at shorter far-UV wavelengths corresponding to redshifted He II $\lambda 304$, the strength of the average cumulative Lyman continuum absorption out to $z \gtrsim 3$ is such that our observations are still consistent with luminous quasars being intrinsically strong emitters in the extreme ultraviolet. In particular, we have used the statistics for the cumulative absorption process derived by Møller & Jakobsen (1990) to show that, given our sensitivity and assuming that the optical power-law spectra of our targets can be extrapolated to shorter wavelengths, the probability of not detecting any object at redshifted He II $\lambda 304$ in 12 attempts is of order $p_B \simeq 30\%$.

Given this low level of significance, it follows that more high-redshift quasars need to be observed in the far-UV before any firm conclusions concerning the prospects for carrying out observations of He II $\lambda 304$ with *HST* can be drawn. In the near future we hope to observe an additional 15 selected $z_{em} > 3$ quasars, thereby more than doubling the sample size of our survey. There is at present no compelling reason to believe that these and other searches will not eventually yield a few moderately absorbed high-redshift quasars whose spectra extend down to He II $\lambda 304$. However, such detections may well take place at flux levels well below $F_\lambda \simeq 5 \times 10^{-16}$ ergs s^{-1} cm^{-2} Å^{-1}, in which case detailed spectroscopic follow-up observations of He II $\lambda 304$ may have to await the further increase in sensitivity promised by the next generation of *HST* spectrographs.

D. Baxter, P. Greenfield, R. Jedrzejewski, and W. B. Sparks acknowledge support from ESA through contract 6500/85/NL/SK. J. C. Blades, P. Crane, and I. R. King acknowledge support from NASA through contracts NAS5-1733, NAS5-27760, and NAS5-28086. G. Weigelt acknowledges support from the German Space Agency (DARA) through contract 50 OR 9204.

APPENDIX

The so-called "proximity effect" seen in the redshift distribution of the Lyman forest lines is widely interpreted to imply that absorption-line systems at high redshifts are kept highly photoionized by a diffuse energetic ($I_\nu \propto \nu^{-\alpha}$, $\alpha \simeq 0.6$) metagalactic flux of intensity $I^0_{\nu_{H\,I}} \approx 10^{-21}$ ergs s^{-1} cm^{-2} sr^{-1} Hz^{-1} at the Lyman limit (Carswell et al. 1982; Murdoch et al. 1986; Bajtlik, Duncan, & Ostriker 1988; Lu, Wolfe, & Turnshek 1991). That the gas is photoionized is also implied by the large $b \simeq 30$ km s^{-1} velocity width of the Lyman forest lines, which corresponds to gas temperature of $T \simeq 5 \times 10^4$ K. Although the origin of the ionizing flux is uncertain (Bechtold et al. 1987b; Miralda-Escudé & Ostriker 1990; Madau 1992), since high ionization species such as C IV and Si IV are commonly seen in other quasar absorption systems containing heavy elements, it is likely that the ionizing spectrum extends to energies of at least ≈ 50 eV; i.e., well above the ionization potentials of neutral and once ionized helium (Steidel & Sargent 1989; Steidel 1990).

The absolute intensity of the ionizing background, combined with the typical sizes of $D \approx 10$ kpc and corresponding neutral hydrogen densities of $n_{H\,I} \approx 10^{-8}$ cm^{-3} for the Lyman forest clouds derived from the study of correlated absorption in close quasar pairs, implies that the optically thin Lyman forest clouds are subject to a very high ionization parameter: $U \simeq (4\pi/hc\alpha)(I^0_{\nu H\,I}/n_H) \approx 10^{-1}$, (e.g., Sargent et al. 1980; Carswell 1988). In this limit where the hydrogen and helium is nearly completely ionized, standard photoionization theory (Osterbrock 1989) leads to the following simple expressions for the relative ionization levels of hydrogen and

helium:

$$\left[\frac{\text{H I}}{\text{H}}\right] \simeq \frac{1}{U}\left(\frac{\alpha_{\text{H I}}}{c\sigma^0_{\text{H I}}}\right)\left[\frac{\alpha+3}{\alpha}\right], \tag{A1}$$

$$\left[\frac{\text{He II}}{\text{He}}\right] \simeq \frac{1}{U}\left(\frac{\alpha_{\text{He II}}}{c\sigma^0_{\text{He II}}}\right)\left[\frac{\alpha+3}{\alpha}\right]\left(\frac{\nu_{\text{He II}}}{\nu_{\text{H I}}}\right)^{\alpha}, \tag{A2}$$

$$\left[\frac{\text{He I}}{\text{He}}\right] \simeq \left[\frac{\text{He II}}{\text{He}}\right]\frac{1}{U}\left(\frac{\alpha_{\text{He I}}}{c\sigma^0_{\text{He I}}}\right)\left[\frac{\alpha+3}{\alpha}\right]\left(\frac{\nu_{\text{He I}}}{\nu_{\text{He I}}}\right)^{\alpha}, \tag{A3}$$

where α is the spectral index of the ionizing flux and $\alpha_{\text{H II}}$, $\alpha_{\text{He I}}$, $\alpha_{\text{He II}}$ and $\sigma^0_{\text{H I}}$, $\sigma^0_{\text{He I}}$ $\sigma^0_{\text{He II}}$ are the H I, He I, and He II recombination coefficients and photoionization cross sections at threshold. For the anticipated values of $U \sim 10^{-1}$ and $\alpha \sim 1$ these equations predict [H I/H] $\sim 10^{-4}$, [He I/He] $\sim 10^{-6}$, and [He II/He] $\sim 10^{-2}$. The ions giving rise to observable absorption, H I, He I and He II, are therefore believed to represent only a minor fraction of the total mass present in the Lyman forest clouds.

The anticipated strengths of the observable absorption in He I and He II can be estimated by scaling to the measured absorption in Lyα. The ratio of the density of neutral helium to neutral hydrogen in an optically thin forest cloud is given by

$$\left[\frac{\text{He I}}{\text{H I}}\right] \simeq \left[\frac{\text{He}}{\text{H}}\right]\left[\frac{\text{He II}}{\text{He}}\right]\left(\frac{\alpha_{\text{He II}}}{\alpha_{\text{H II}}}\right)\left(\frac{\sigma^0_{\text{H I}}}{\sigma^0_{\text{He I}}}\right)\left(\frac{\nu_{\text{He I}}}{\nu_{\text{H I}}}\right)^{\alpha} \approx 0.1 \times 1.8^{\alpha}\left[\frac{\text{He II}}{\text{He}}\right], \tag{A4}$$

where $(\alpha_{\text{He II}}/\alpha_{\text{H II}}) \simeq 1.2$, $(\sigma^0_{\text{H I}}/\sigma^0_{\text{He I}}) \simeq 1$, and [He/H] $\simeq 0.1$ is the standard big bang helium to hydrogen ratio by number.

Equation (A4) predicts that the abundance of neutral helium in the Lyα forest clouds should be far lower than that of neutral hydrogen; i.e., [He I/H I] $\sim 10^{-3}$. Absorption in the He I λ584 forest lines is therefore expected to be very weak compared to Lyα—a prediction that has recently been confirmed through *HST* observations of HS 1700+6416 (Reimers et al. 1992). Possible exceptions however, are single dense Lyman limit and damped Lyα systems which are optically thick in the Lyman continuum and are therefore not highly photoionized (Miralda-Escudé & Ostriker 1992).

In contrast, absorption due to once ionized helium is expected to be universally strong. The predicted density ratio of He II to H I in the forest clouds is

$$\left[\frac{\text{He II}}{\text{H I}}\right] \simeq \left[\frac{\text{He}}{\text{H}}\right]\left(\frac{\alpha_{\text{He III}}}{\alpha_{\text{H II}}}\right)\left(\frac{\sigma^0_{\text{H I}}}{\sigma^0_{\text{He II}}}\right)\left(\frac{\nu_{\text{He II}}}{\nu_{\text{H I}}}\right)^{\alpha} \approx 2.4 \times 4^{\alpha}, \tag{A5}$$

where in this case $(\alpha_{\text{He II}}/\alpha_{\text{H III}}) \simeq 6$ and $(\sigma^0_{\text{H I}}/\sigma^0_{\text{He II}}) = 4$. It follows that for an ionizing spectrum with slope in the range, $\alpha \simeq 0.5 - 2$, the column density of once ionized helium through a given Lyman forest cloud is predicted to exceed that of neutral hydrogen by a factor [He II/H I] $\approx$ 5–40. Note that softer photoionizing spectra lead to larger predicted [He II/H I] ratios. If the ionizing background flux does not extend down to the He II photoionization threshold at 54.4 eV, then the relative abundance of He II could be as high as [He II/H I] $\simeq$ [He/H]/[H I/H] $\approx 10^3$.

Since the oscillator strength of the He II λ304 transition is the same as that of Lyα, and the equivalent width of unsaturated lines grows as $W_\lambda \propto N\lambda^2 f$ (Spitzer 1978), the He II λ304 lines of the weaker forest systems will equal or exceed the corresponding Lyα lines in strength if [He II/H I] $\gtrsim$ 16. On the other hand, the He II λ304 equivalent widths of saturated forest systems are likely to be smaller than those of the corresponding Lyα lines due to the expected factor 2 lower thermal line widths of the helium ion. However, since the density of lines per wavelength interval is a factor 4 higher in the He II λ304 forest because of the shorter wavelength, the net line blanketing in the He II forest could easily exceed that of H I in total strength. At emitted wavelengths $\lambda \leq 228$ Å below the He II photoionization edge, intense He II continuum absorption should be also present. Since this absorption is not prone to saturation effects, it will almost certainly be stronger than that of neutral hydrogen.

The above predictions for the ionization levels of hydrogen and helium in the Lyman forest clouds are equally valid for the ambient intergalactic medium, since such a medium will be of lower density than the forest clouds, and therefore have a correspondingly higher ionization parameter. The best limit on the optical depth of any redshift-smeared H I Lyα Gunn-Peterson trough at high redshift is $\tau_{\text{H I}} \lesssim 0.02 \pm 0.03$, corresponding to $\approx$10% of the total blanketing of the forest (Steidel & Sargent 1987). The optical depth of the matching He I λ584 trough is therefore expected to be far too small to be observable; i.e., $\tau_{\text{He I}} \simeq 0.31$[He I/H I]$\tau_{\text{H}} \lesssim 10^{-4}$. This is consistent with the fact that no evidence for He I trough absorption has been detected to date in the few high-redshift quasars bright enough to be reached with *IUE* (Green et al. 1980; Reimers et al. 1989; Tripp, Green, & Bechtold 1990) or observed so far with *HST* (Beaver et al. 1991; Reimers et al. 1992).

On the other hand, it is entirely possible that an ambient intergalactic medium having an equivalent He II λ304 Gunn-Peterson trough depth as high as $\tau_{\text{He II}} \simeq 0.25$[He II/H I]$\tau_{\text{H I}} \sim 1$ could exist. In fact, if such He II absorption is detected, then the main problem will be to distinguish the smooth Gunn-Peterson absorption trough from the anticipated intense He II forest line blanketing.

REFERENCES

Antonucci, R. R. J., Kinney, A. L., & Ford, H. C. 1989, ApJ, 342, 64
Bahcall, J. N., et al. 1993, ApJS, 87, 1
Bajtlik, S., Duncan, R. C., & Ostriker, J. P. 1988, ApJ, 327, 570
Barthel, P. D., Tytler, D. R., & Thompson, B. 1990, A&AS, 82, 339
Beaver, E. A., Burbidge, E. M., Cohen, R., Junkkarinen, V., Lyons, R., & Rosenblatt, E. 1992, in Science with the *Hubble Space Telescope*, ed. P. Benvenuti & E. Schreier (Garching: ESO), 53
Beaver, E. A., et al. 1991, ApJ, 377, L9

Bechtold, J., Czerny, B., Elvis, M., Fabbiano, G., & Green, R. F. 1987a, ApJ, 314, 699
Bechtold, J., Green, R. F., Weymann, R. J., Schmidt, M., Estabrook, F. B., Sherman, R. D., Wahlquist, H. D., & Heckman, T. M. 1984, ApJ, 281, 76
Bechtold, J., Weymann, R. J., Lin, Z., & Malkan, M. A. 1987b, ApJ, 315, 180
Bohlin, R. C., Turnshek, D. A., Williamsson, R. L., Lupie, O. L., Koornneef, J., & Morgan, D. H. 1990, AJ, 99, 1243
Burrows, C. J., Holtzman, J. A., Faber, S. M., Bely, P. Y., Hasan, H., Lynds, C. R., Schroeder, D. 1991, ApJ, 369, L21
Carswell, R. F. 1988, in QSO Absorption Lines, Probing the Universe, ed. J. C. Blades, D. Turnshek, & C. A. Norman (Cambridge: Cambridge Univ. Press), 91
Carswell, R. F., Strittmatter, P. A., Williams, E. E., Beaver, E. A., & Harms, R. 1975, ApJ, 195, 269
Carswell, R. F., Whelan, J. A. J., Smith, M. G., Boksenberg, A., & Tytler, D. 1982, MNRAS, 198, 91
Courvoisier, T. J. L., & Clavel, J. 1991, A&A, 248, 389
Davidson, K., & Netzer, H. 1979, Rev. Mod. Phys., 51, 715
Edelson, R. A., & Malkan, M. A. 1986, ApJ, 308, 59
Elvis, M., Giommi, P., Wilkes, B. J., & McDowell, J. 1991, ApJ, 378, 537
Green, R. F., Pier, J. R., Schmidt, M., Estabrook, F. B., Lane, A. L., & Wahlquist, H. D. 1980, ApJ, 239, 483
Greenfield, P., et al. 1991, Space Astronomical Telescopes and Instruments, Proc. SPIE, 1494, 16
Gunn, J. E., & Peterson, B. A. 1965, ApJ, 142, 1633
Hunstead, R. W. 1988, in QSO Absorption Lines, Probing the Universe, ed. J. C. Blades, D. Turnshek, & C. A. Norman (Cambridge: Cambridge Univ. Press), 71
Ikeuchi, S., & Ostriker, J. P. 1986, ApJ, 301, 522
Jakobsen, P., Greenfield, P., & Jedrzejewski, R. 1992, A&A, 253, 329
Khare, P., York, D. G., & Green, R. 1989, ApJ, 347, 627
Kinney, A. L., Bohlin, R. C., Blades, J. C., & York, D. G. 1991, ApJS, 75, 645
Lanzetta, K. M. 1988, ApJ, 332, 96
Laor, A., & Netzer, H. 1989, MNRAS, 238, 897
Lu, L., Wolfe, A. M., & Turnshek, D. A. 1991, ApJ, 367, 19
Madau, P. 1988, ApJ, 327, 116
———. 1992, ApJ, 389, L1
Miralda-Escudé, J., & Ostriker, J. P. 1990, ApJ, 350, 1
———. 1992, ApJ, 392, 15
Morton, D. C., Peterson, B. A., Jian-Sheng, C., Wright, A. E., & Jauncey, D. L. 1989, MNRAS, 241, 595
Møller, P., & Jakobsen, P. 1990, A&A, 228, 299
Murdoch, H. S., Hunstead, R. W., Pettini, M., & Blades, J. C. 1986, ApJ, 309, 19
O'Brien, P. T., Gondhalekar, P. M., & Wilson, R. 1988, MNRAS, 233, 801
Oke, J. B., & Korycansky, D. G. 1982, ApJ, 255, 11
Osmer, P. S. 1979, ApJ, 227, 18
Osterbrock, D. E. 1989, Astrophysics of Gaseous Nebulae and Active Galactic Nuclei (Mill Valley: University Science Books), 23
Paresce, F. 1992, Faint Object Camera Instrument Handbook (Baltimore: STScI)
Peterson, B. A., Wright, A. E., Jauncey, D. L., & Condon, J. J. 1979, ApJ, 47, 401
Reimers, D., Clavel, J., Groote, D., Engels, D., Hagen, H. J., Naylor, T., Wamsteker, W., & Hopp, U. 1989, A&A, 218, 71
Reimers, D., Vogel, S., Hagen, H. J., Engels, D., Groote, D., Wamsteker, W., Clavel, J., & Rosa, M. R. 1992, Nature, 360, 561
Robertson, J. G. 1986, PASP, 98, 1220
Sargent, W. L. W. 1988, in QSO Absorption Lines, Probing the Universe, ed. J. C. Blades, D. Turnshek, & C. A. Norman (Cambridge: Cambridge Univ. Press), 1
Sargent, W. L. W., Boksenberg, A., & Steidel, C. C. 1988, ApJS, 68, 639
Sargent, W. L. W., Steidel, C. C., & Boksenberg, A. 1989, ApJS, 69, 703
Sargent, W. L. W., Young, P. J., Boksenberg, A., & Tytler, D. 1980, ApJS, 42, 41
Savage, B. D., & Mathis, J. S. 1979, ARA&A, 17, 73
Sciama, D. W. 1988, MNRAS, 230, 13P
Sherman, R. D. 1982, ApJS, 256, 370
Smith, M. G., et al. 1981, MNRAS, 195, 437
Spitzer, L. 1978, Physical Processes in the Interstellar Medium (New York: Wiley), 52
Stark, A. A., Gammie, C. F., Bally, J., Linke, R. A., Heiles, C., & Hurwitz, M. 1992, ApJS, 79, 77
Steidel, C. C. 1990, ApJS, 72, 1
Steidel, C. C., & Sargent, W. L. W. 1987, ApJ, 318, L11
———. 1989, ApJ, 343, L33
Tripp, T. M., Green, R. F., & Bechtold, J. 1990, ApJ, 364, L29
Turnshek, D. A., Wolfe, A. M., Lanzetta, K. M., Briggs, F. H., Cohen, R. D., Foltz, C. B., Smith, H. E., & Wilkes, B. J. 1989, ApJ, 344, 567
Tytler, D. 1982, Nature, 298, 427
Whelan, J. A. J., Smith, M. G., & Carswell, R. F. 1979, MNRAS, 189, 363
Wilkes, B. J. 1984, MNRAS, 207, 73
Willinger, G. M., Carswell, R. F., Webb, J. K., Boksenberg, A., & Smith, M. G. 1989, MNRAS, 237, 635
Wilson, R., Carnochan, D. J., & Gondhalekar, P. M. 1979, Nature, 277, 457
Wolfe, A. M., Turnshek, D. A., Smith, H. E., & Cohen, R. D. 1986, ApJS, 61, 249